PERGAMON

Robotics and Computer Integrated Manufacturing 17 (2001) 215–222

Robotics and Computer Integrated Manufacturing

www.elsevier.com/locate/rcim

Optimal shape error analysis of the matching image for a free-form surface

Kuang-Chao Fan[a,*], Tung-Hsien Tsai[b]

[a]Department of Mechanical Engineering, National Taiwan University, 1, Roosevelt Rd., Sec. 4, Taipei 10617, Taiwan, ROC
[b]Department of Mechanical Engineering, Shu-Teh Junior College of Technology and Commerce, 11, Dah-ching St., Sec. 2, Taichung, Taiwan, ROC

Received 1 April 2000; received in revised form 24 August 2000; accepted 15 September 2000

Abstract

When using an optical non-contact scanning system to measure an object that has a large surface, large curvature, or a full 360° profile, one can acquire only one set of sectional measurement points each time. For reconstructing the entire object, every set of sectional measurement points acquired at different positions must match. Therefore, the optimal shape error analysis for the matching image of two or more sets of sectional measurement points is desired. This paper presents a measurement system that combines two CCD cameras, one line laser and a three-axis motion stage. It forms an optical non-contact scanning system in association with the mathematical method of direct shape error analysis for the use in reverse engineering. This analysis and measurement system can be used for the profile measurements of free-form objects. It analyzes the matching image of a free-form surface with high efficiency and accuracy. The validity and applicability of this system are demonstrated by two practical examples.

Keywords: Reverse engineering; Shape error; Surface fitting; Image matching; Optimization

1. Introduction

Optical non-contact scanning measurement systems have been widely used in reverse engineering for rapid product prototyping in recent years. Because it is flexible and quick, it can be used for profile measurement of objects with complex surfaces. However, when measuring an object that has a large surface, large curvature, or a full 360° profile, one can acquire only one set of sectional measurement points in each measurement. For reconstructing the entire object, every set of sectional measurement points acquired at different positions must match. Therefore, the optimal shape error analysis for the matching images of the same area for two sets of sectional measurement surfaces is desired.

Some approaches for registering and building three-dimensional (3-D) models from multiple range images have been developed in recent years [1–7]. However, the goal of the new approach is to develop an algorithm that has high efficiency and accuracy. In general, there is no existing absolute reference surface when matching every set of sectional measurement surfaces. Therefore, this study has determined the first set of sectional measurement surfaces to be a matching reference surface. In this article, an analysis and measurement system is proposed. It combines an optical non-contact scanning measurement system using two CCD cameras with a direct shape error analysis approach. This system can be used for the profile measurement of a large object and can analyze the matching image of a free-form surface with high efficiency and accuracy.

2. Triangulation measurement

The principle of triangulation measurement with one camera is shown in Fig. 1. In the figure, $P(x, y, z)$ is a point in the world coordinate (X, Y, Z) and $P'(u, v)$ is its focused point in the image plane (U, V). According to the geometrical optics and similar triangles, the coordinates of point

* Corresponding author. Tel.: +886-2-2362-0032; fax: +886-2-2364-1186.
E-mail address: fan@ccms.ntu.edu.tw (K.-C. Fan).

0736-5845/01/$ - see front matter
PII: S0736-5845(00)00029-6

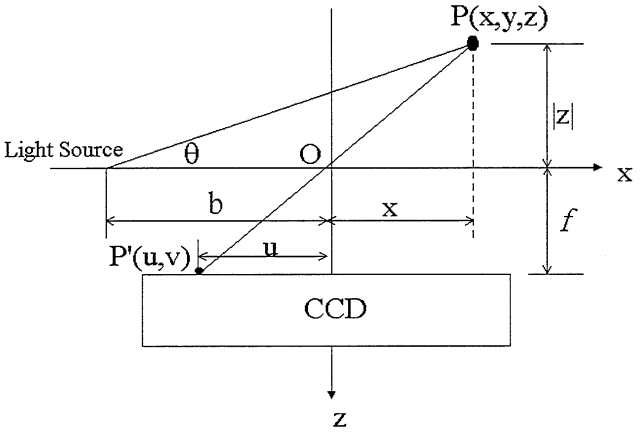

Fig. 1. The principle of triangulation measurement.

$P(x, y, z)$ can be calculated by

$$\frac{f}{u} = \frac{|z|}{x}, \tag{1}$$

$$\frac{b + x}{|z|} = \cot\theta, \tag{2}$$

where f is the focal length, θ is the angle between the X-axis and light direction, and b is the distance between the light source and the lens's optical center O.

From Eqs. (1) and (2), we can get

$$x = \frac{bu}{f\cot\theta - u}. \tag{3}$$

Similarly, in the Y-direction we have

$$\frac{f}{v} = \frac{|z|}{y} \quad \text{and} \quad \frac{x}{y} = \frac{u}{v},$$

which yield

$$y = \frac{bv}{f\cot\theta - u}, \tag{4}$$

$$z = \frac{-bf}{f\cot\theta - u}. \tag{5}$$

Therefore, the coordinates of point $P(x, y, z)$ are

$$\left(\frac{bu}{f\cot\theta - u}, \frac{bv}{f\cot\theta - u}, \frac{-bf}{f\cot\theta - u}\right).$$

Triangulation measurement is one of the popular measurement techniques. It has advantages in fast computation and easy operation. However, it possesses disadvantages in complicated calibration of system parameters and tedious system set-up. In practice, inaccuracy in system parameters and system set-up will induce large measurement errors.

3. The optical non-contact scanning measurement system

In principle, the one CCD camera system can grab the projected line image on the surface and fit a free-form line at a time. Having scanned the whole image, the entire free-form surface profile of the object can be constructed. In practice, the one CCD camera cannot always successfully capture the line image at each position because the inspected surface may have steep slopes and protruded profiles. In order to solve this problem, this study developed a measurement system using two CCD cameras to collect image information. The cameras are located on both sides of the laser diode so that more image information is obtained and compensated for the loss of data that resulted from using only one CCD camera. Fig. 2 shows the schematic diagram of the constructed scanning measurement system. The optical detector is composed of two CCD cameras and a line laser diode, and is mounted on a linear stage. As the laser diode projects a laser stripe onto the object, the two CCD cameras detect the deformed laser line image simultaneously. Between the two image data collected the clearer one will be stored. By stepping the optical detector to prescribed positions, a series of deformed line images can be collected. Consequently, the entire image information for an object is acquired using this optical scanning system.

3.1. System set-up for parameters calibration

Fig. 3 shows the experimental set-up for the CCD system. A laser strip is projected onto the standard template, and the CCD cameras detect the line image. The template was made using a laser writer with 1 μm

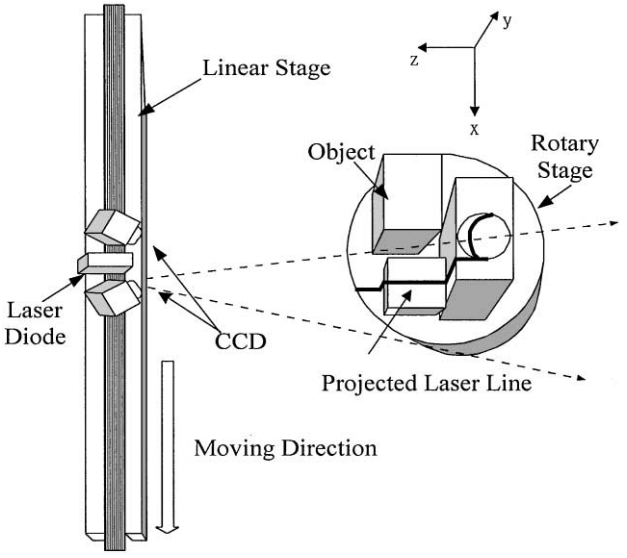

Fig. 2. Schematic diagram of the proposed optical scanning measurement systems.

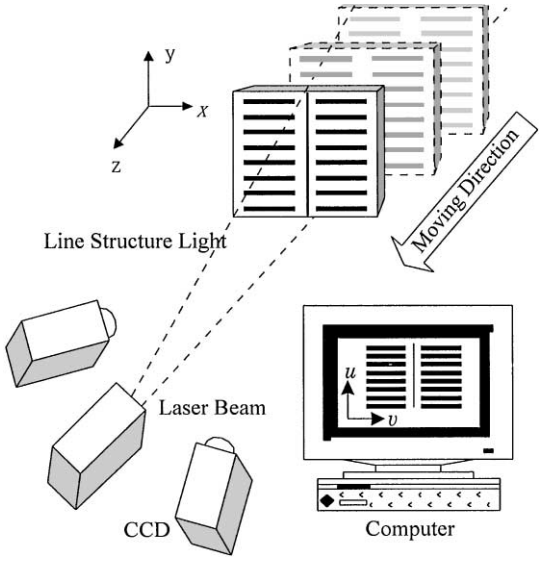

Fig. 3. Experimental set-up for parameters calibration.

accuracy of line spacing. Since the distance between each horizontal line on the standard template is known, the intersection point between each horizontal line and vertical laser line stripe indicates the (Y, Z) coordinate of the space plane. The standard template is successively moved step-by-step along the Z-axis direction. The CCD cameras can grab the image of those points with respect to several space planes, respectively. The two-dimensional (2-D)-measurement information in the image plane can be transformed into its space position using the least-squares mapping algorithm described as follows.

3.2. Coordinate mapping principle

Let (Y_k, Z_k) be a coordinate of the standard template in the space position, and (U_k, V_k) be the corresponding coordinate in the image plane. Then, a mapping algorithm can be established using the least-squares polynomial function [8].

$$Y(U,V) = \sum_{j=0}^{N} \sum_{i=0}^{N-j} C_{Y_{ij}} U^i V^j, \tag{6}$$

$$Z(U,V) = \sum_{j=0}^{N} \sum_{i=0}^{N-j} C_{Z_{ij}} U^i V^j, \tag{7}$$

where $C_{Y_{ij}}$ and $C_{Z_{ij}}$ are the coefficients of the polynomial mapping functions.

The related error functions E_Y and E_Z of $Y(U,V)$ and $Z(U,V)$, respectively, can be obtained by

$$E_Y = \sum_{k=0}^{N} (Y_k - Y)^2, \quad E_Z = \sum_{k=0}^{N} (Z_k - Z)^2. \tag{8}$$

Therefore, the coefficients $C_{Y_{ij}}$ and $C_{Z_{ij}}$ can be determined from the minimum error

$$\frac{\partial E_Y}{\partial C_{Y_{ij}}} = 0, \quad \frac{\partial E_Z}{\partial C_{Z_{ij}}} = 0. \tag{9}$$

From Eqs. (6) and (7), one can obtain the related space coordinate for each measurement data on the image plane. The corresponding space coordinate (Y, Z) for each pixel position (U, V) of the laser beam image in the CCD plane can be determined. Hence, the entire profile can be formed by the integration of the scanned data.

4. The direct shape error analysis method

The construction of the surface measurement points can be determined by several approaches [9–12]. This paper adopted the bicubic uniform B-spline interpolation approach to describe the first set measurement points, and to reconstruct multiple surface patches. These multiple bicubic B-spline patches must pass through all measurement points of the first set and match their boundaries with C^0 and C^1 continuity. Therefore the accuracy in this surface reconstruction step is guaranteed. The shape error of the matching image of the free-form surface in this paper is defined as the maximum value of the nearest distances from the second set measurement points to the reference (the first set) surface. Obviously, the objective function of shape error analysis is the sum of the squared nearest distances. In general, an iterative method algorithm for finding the nearest distance is widely used [16]. This method is, however, time consuming and tedious for finding the convergence solution. Zhang [13] proposed iterative algorithm for finding the closest point for registration of free-form curves and surfaces. Bergevin et al. [14] employed least-squares estimation to minimize the nearest distance. Eggert et al. [15] adopted *k–d* tree algorithm for searching the closest point. Ho [19] employed Powell's iterative searching method to find the corresponding point in the reference surface having the shortest distance from each of the second set measurement point. This algorithm is called the inverse method. In this study, an improved algorithm, which is called the direct method, was proposed.

For finding the nearest distance between the second set measurement points and the reference surface, the direct method solves the intersection between the reference surface normal vector and the second set measurement point directly. Fig. 4 shows the direct method concept for finding the nearest distance. Based on this concept, a detailed algorithm of the direct method is described as follows:

Let $q_{ij} = [x_{mij}, y_{mij}, z_{mij}]^{\mathrm{T}}$ be the measurement points of the second set, and $p_{ij} = [x_{rij}, y_{rij}, z_{rij}]^{\mathrm{T}}$ be the parametric representation point of the ijth B-spline patch in

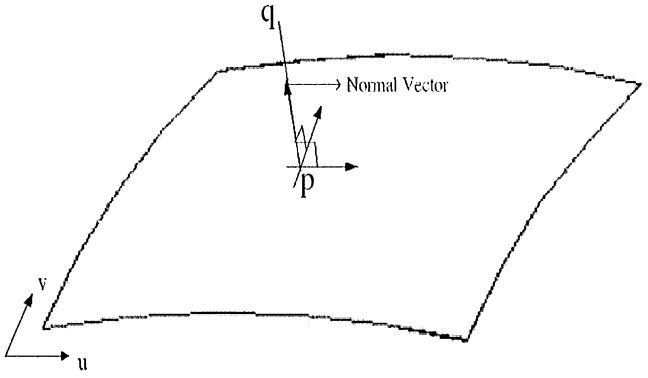

Fig. 4. The direct method concept for finding the nearest distance.

the reference surface. Then the nearest distance between the second set measurement point and the reference surface can be determined by solving the following two non-linear equations:

$$F_1(u,v) = (x_{mij} - x_{rij})\frac{\partial x_{rij}}{\partial u} + (y_{mij} - y_{rij})\frac{\partial y_{rij}}{\partial u} + (z_{mij} - z_{rij})\frac{\partial z_{rij}}{\partial u} = 0, \quad (10)$$

$$F_2(u,v) = (x_{mij} - x_{rij})\frac{\partial x_{rij}}{\partial v} + (y_{mij} - y_{rij})\frac{\partial y_{rij}}{\partial v} + (z_{mij} - z_{rij})\frac{\partial z_{rij}}{\partial v} = 0. \quad (11)$$

Using the Newton–Raphson Method [17], the solution to the above equations can be determined by solving the following matrix equations. The process is repeated until the deviation converges to a required value.

$$\mathbf{F}(u_k, v_k) + \mathbf{J}(u_k, v_k)\mathbf{Z}_k = 0, \quad (12)$$

where

$$\mathbf{F}(u_k, v_k) = \begin{bmatrix} F_1(u_k, v_k) \\ F_2(u_k, v_k) \end{bmatrix}, \quad \mathbf{Z}_k = \begin{bmatrix} u_{k+1} - u_k \\ v_{k+1} - v_k \end{bmatrix}$$

and the Jacobian matrix

$$\mathbf{J}(u_k, v_k) = \begin{bmatrix} \dfrac{\partial F_1(u_k, v_k)}{\partial u} & \dfrac{\partial F_1(u_k, v_k)}{\partial v} \\ \dfrac{\partial F_2(u_k, v_k)}{\partial u} & \dfrac{\partial F_2(u_k, v_k)}{\partial v} \end{bmatrix}.$$

From the direct method description, one can realize that the computing time for finding the nearest distance is faster than the iterative method. The highlight of this paper is to use the direct method to find the nearest distance between the second set measurement point and the reference surface, which reduces the computation time. From the applied examples, the computing time for this approach was reduced by about 82–92% when compared with the inverse method.

5. Initial localization and optimization

In general, there is no existing absolute reference point between the two sets of measurement data when measuring an object. This study determined the initial geometric matching location of the two sets of measurement data using human–computer interaction. Fig. 5 shows the two sets of sectional measurement data of a car model with a complex surface taken from different measurement angles. The initial two sets of sectional measurement data were located using coordinate translations and rotations as shown in Fig. 6.

When the initial sets were located, the initial shape error and initial parameters of a rigid-body transformation of the two sets of sectional measurement data were obtained. The accuracy of the shape error would certainly not satisfy our requirements. Thus, according to the direct method, the least-squares method and optimization algorithm, an optimal shape error analysis approach

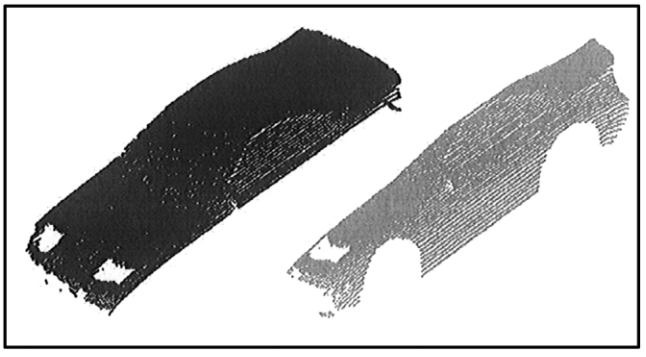

Fig. 5. Two sets of sectional measurement data for a car model with a complex surface taken from different measurement angles.

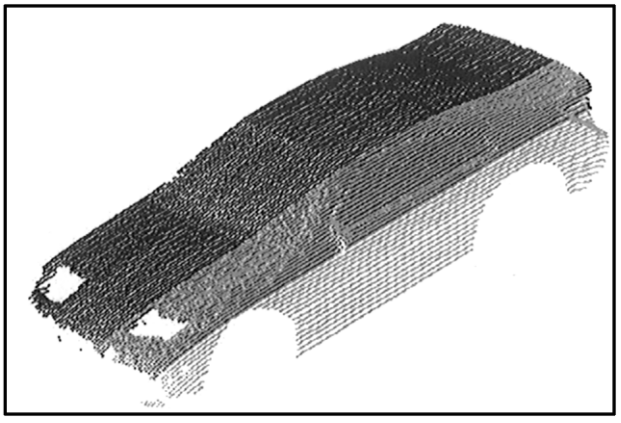

Fig. 6. The initial mapping of two-sectional measurement data using coordinate translations and rotations.

is proposed. It can determine the optimal results of the matching image. The least-squares method and optimization algorithm are described as follows:

Let $(x, y, z, \alpha, \beta, \gamma)$ be the parameters of a rigid-body transformation and $d_1, d_2, d_3, \ldots, d_n$ be the nearest distances between the second set measurement points q_i $(i = 1 - n)$ and the reference surface, respectively. The objective function is defined as the sum of the squared nearest distances.

$$F(x, y, z, \alpha, \beta, \gamma) = \sum_{i=1}^{n} [d_i(x, y, z, \alpha, \beta, \gamma)]^2, \qquad (13)$$

where (x, y, z) are the linear translations of a rigid-body transformation in the three coordinate directions and (α, β, γ) are the angular rotations of a rigid-body transformation with respect to the three coordinate axes. The shape error analysis of a measured 3-D surface involves searching for the six variables $(x, y, z, \alpha, \beta, \gamma)$ so that the objective function is minimized.

When applying the shape error analysis of a measured line, the design variables would be reduced to three, namely (x, y, α). In this study, the DFPM algorithm (Davidon–Fletcher–Powell Method) was adopted [18]. Based on the construction of a B-spline surface and the DFPM algorithm, this work developed a computer program to analyze the shape error of measured data with respect to the reference surface. It is called the direct shape error analysis method (DSEAM). The flow chart for the DSEAM is shown in Fig. 7. The slave data is moved to the blending area of the master data by the initial variables $(x_0, y_0, z_0, \alpha_0, \beta_0, \gamma_0)$. The DFPM algorithm then searches the optimum variables so that the objective function is minimized.

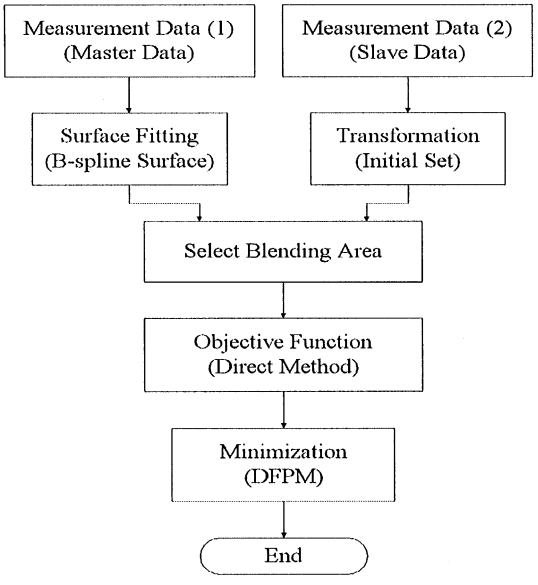

Fig. 7. The DSEAM flow chart for the matching free-form surface image.

6. Application examples

6.1. Example 1: a large free-form surface

Because the optical detector was mounted on the linear stage, if the dimension of the object is larger than the linear stage range, we must divide the object into several parts and measure it progressively. Fig. 8 shows the two sets of measurement points for a large free-form surface, which was divided by two sections between which there was an unknown overlapping area. The initial two sets of measurement points were partially matched by approximation using human–computer interaction. We then selected the blending area for optimal shape error analysis of the matching image, as shown in Fig. 9. In this case, there were 793 points in the matching image area.

The optimal shape error results and the optimal parameters of a rigid body transformation using the DSEAM are shown in Table 1. The optimal shape error is 0.3334 mm, which is reduced by 7 μm when compared to the initial shape error. Fig. 10 shows an enlarged error diagram of the line segments at optimal condition. The selected zone is again enlarged in Fig. 11. Fig. 12 shows the complete shape of this large free-form surface after shape error analysis. The computation time was reduced by about 92% when compared with the inverse method.

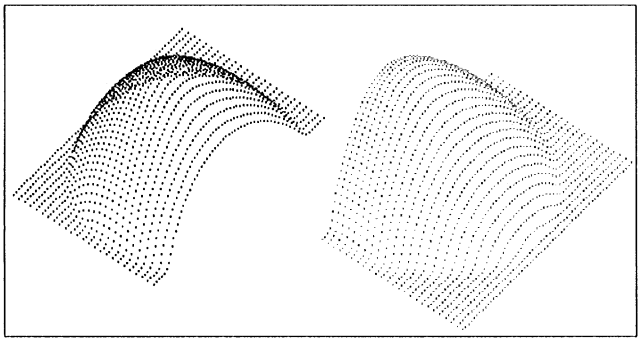

Fig. 8. The two sets of measurement points of a large free-form surface.

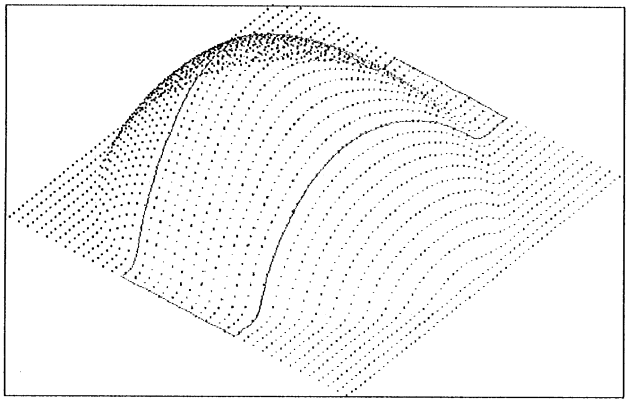

Fig. 9. The area for optimal shape error analysis of the matching image for a large free-form surface.

Table 1
The results of optimal shape error analysis of a large free-form surface

DSEAM	
Initial set	Optimal blending set
x −0.050 mm	x −0.0482 mm
y 35.999 mm	y 35.9712 mm
z 0.010 mm	z 0.0095 mm
α 0 rad	α −0.000662 rad
β 0 rad	β −0.004135 rad
γ 0 rad	γ 0.001124 rad
Initial shape error	0.3405 mm
Optimal shape error	0.3334 mm
Computing time	19.430 s

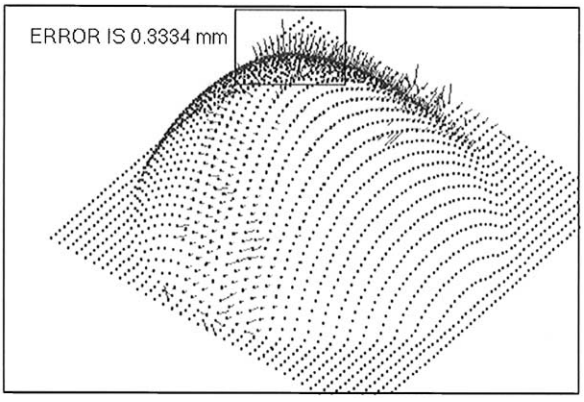

Fig. 10. The enlarged diagram of optimal shape error of selected line segments.

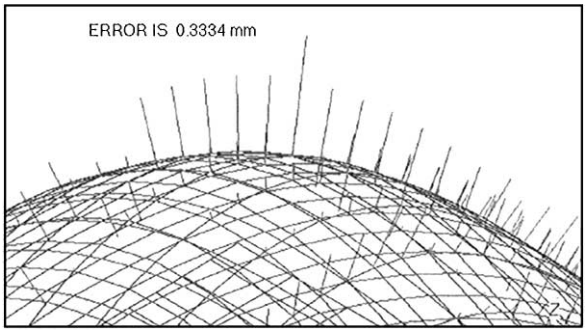

Fig. 11. The local enlargement of the line segments of optimal shape error.

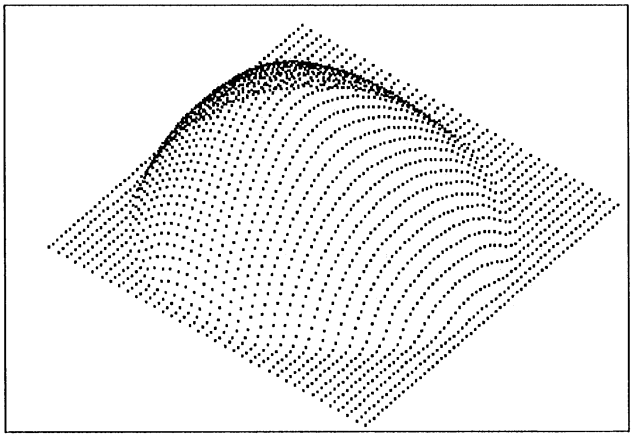

Fig. 12. The complete measured shape of the large free-form surface.

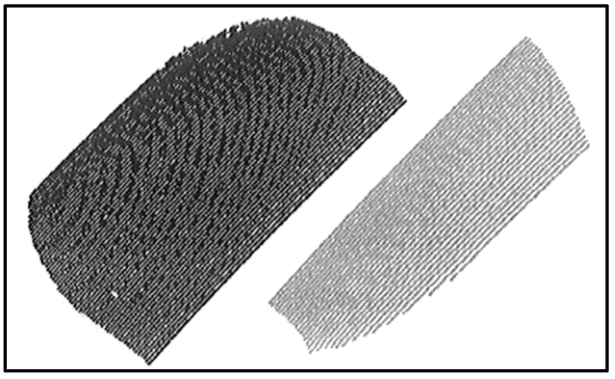

Fig. 13. Two sets of measurement points for a car rear-view mirror case.

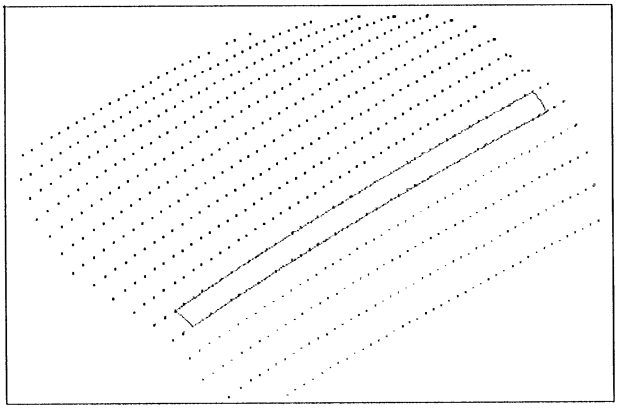

Fig. 14. The area of optimal shape error analysis for a car rear-view mirror case.

6.2. *Example 2*: *a car rear-view mirror case*

For an object having large curved surface, the sectional measurement points will be obtained from different measurement angles. Fig. 13 shows the two sets of measurement points of a car rear-view mirror case, which were taken from different measurement angles. The initial mapping of the second set data to the first set data was located using human–computer interaction. The area for optimal shape error analysis of the matching image was then selected, as shown in Fig. 14. In this case, there were 2880 points in the area of the matching image. Fig. 14, however, shows only a reduced data set.

Table 2
The results of optimal shape error analysis of a car rear-view mirror case

DSEAM	
Initial set	Optimal blending set
x −0.528 mm	x −0.5303 mm
y 50.000 mm	y 49.8268 mm
z 0.200 mm	z 0.0479 mm
α 0.139712 rad	α 0.133798 rad
β 0 rad	β 0.053395 rad
γ 0 rad	γ 0.005709 rad
Initial shape error	0.6849 mm
Optimal shape error	0.4664 mm
Computing time	273.925 s

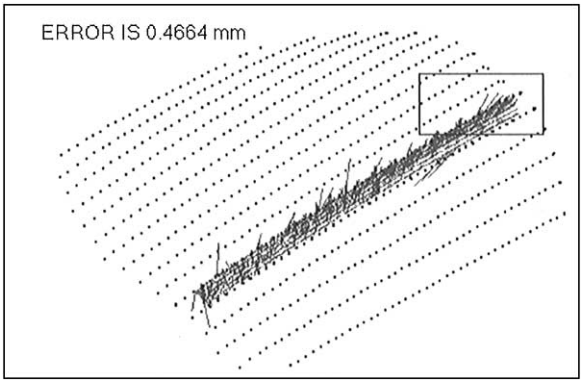

Fig. 15. The line segments of the optimal shape error for a car rear-view mirror case.

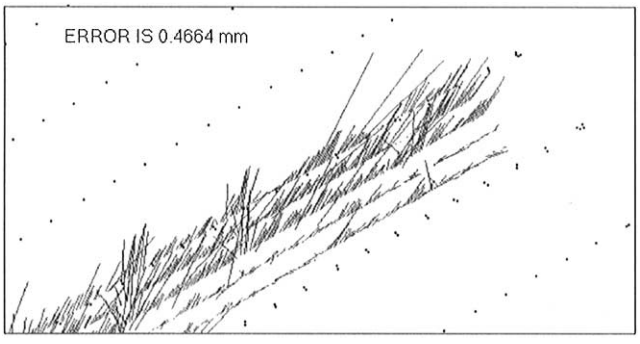

Fig. 16. The local enlargement of the line segments for the optimal shape error of a car rear-view mirror case.

The optimal shape error results and the optimal parameters of a rigid body transformation using the DSEAM are shown in Table 2. The optimal shape error is 0.4664 mm, which is reduced by 219 μm when compared with the initial shape error. Fig. 15 shows the enlargement of the line segments of the optimal shape error. The local enlargement of the selected line segments of the optimal shape error is shown in Fig. 16. Fig. 17 shows the complete shape of this object. The computation time was reduced by about 82% when compared with the inverse method.

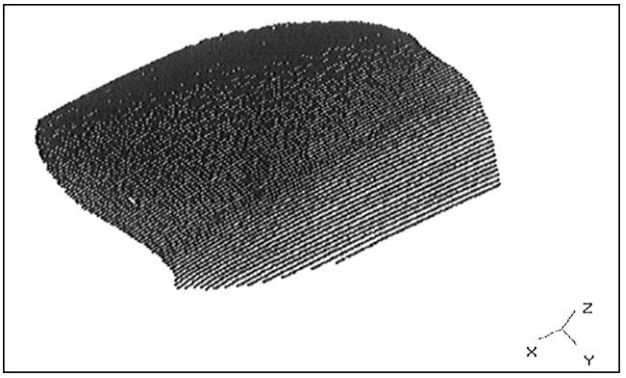

Fig. 17. The complete measured shape of the car rear-view mirror case.

7. Conclusions

Optical non-contact scanning measurement systems have been widely used in reverse engineering for rapid product prototyping in recent years. Because such systems are flexible and quick, they can be used for the profile measurement of objects with complex surfaces.

This paper presented a measurement system, which combines two CCD cameras, one line laser, and a three-axis motion stage to form the optical non-contact scanning system associated with the DSEAM. This measurement system can collect more image information and compensate for the loss of data that resulted from using only one CCD camera. This system can execute the associated analysis for the matching image of a free-form surface with high efficiency and accuracy. The validity and applicability of this measurement system were demonstrated by two practical examples.

References

[1] Shoo KC, Menq CH. Localization of 3-D object having complex sculptured surfaces using tactile sensing and surface description. ASME, J Engng Ind 1991;113:85–92.
[2] Yau HT, Menq CH. Path planning for automated dimension inspection using coordinate measuring machines. Proceedings of the 1991 IEEE International Conference on Robotics and Automation, Sacramento, California, April 1991. p. 1934–9.
[3] Chen Y, Medion G. Object modelling by registration of multiple range images. Image Vision Comput 1992;10(3):145–55.
[4] Blais G, Levine MD. Registering multiview range data to create 3D computer objects. IEEE Trans 1995;17(8):820–4.
[5] Bergevin R, Soucy M, Gagnon H, Lanrendeau D. Towards a general multi-view registration technique. IEEE Trans Pattern Anal Mach Intell 1996;18(5):540–7.

[6] Masuda T, Yokoya N. A robust method for registration and segmentation of multiple range images. Comput Vision Image Understanding 1995;61(3):295–307.
[7] Higuchi K, Hebert M, Ikeuch K. Building 3-D models from unregistered range images. Graphical Models Image Process 1995;57(4):315–33.
[8] Tai WC, Chang M. Non-contact profilometric measurement of large-form parts. Opt Engng 1996;35(9):2730–5.
[9] Beeker E. Smoothing of shapes designed with free-form surface. Comput-Aided Des 1986;18(4):224–32.
[10] Armit AP. Curve and surface design using multipach and multiobject design systems. Comput-Aided Des 1993;25(4): 251–61.
[11] Chen YD, Tang XJ, Ni J, Wu SM. Automatic digitization of free-form curve by coordinate measuring machine. Engineered surface, PED-vol. 62, New York: ASME, 1992. p. 47–59.
[12] Rogers DF, Adams JA. Mathematical elements for computer graphics. New York: McGraw-Hill, 1990.
[13] Zhang Z. Iterative point matching for registration of free-form curves and surfaces. Int J Comput Vision 1994;13(2):119–52.
[14] Bergevin R, Lanrendeau D, Poussart D. Registering range views of multipart objects. Comput Vision Image Understanding 1995;6(1):1–16.
[15] Eggert DW, Fitzgibbon AW, Fisher RB. Simultaneous registration of multiple range views for use in reverse engineering of CAD models. Comput Vision Image Understanding 1998;69(3):253–72.
[16] Wismer DA, Chattergy R. Introduction to nonlinear optimization. Amsterdam: North-Holland, 1978.
[17] Patel VA. Numerical analysis. London: Saunders College, 1994.
[18] Press WH. Numerical recipes in C. Cambridge: Cambridge University Press, 1994. p. 317–28.
[19] Ho CC. 3D Surface matching techniques in image measurements. Master thesis, National Taiwan University, 1997.